https://doi.org/10.5194/essd-2026-518
Preprint. Discussion started: 23 July 2026

Earth System Science Data
Open Access Discussions

Constructing nationally comprehensive annual rice paddy maps for Madagascar from 2017 to 2025

Ryoungseob Kwon[1,2], Youngryel Ryu[1,2,3,4]*, Giacomo De Nicola[5], Hervet Randriamady[5], Oladimeji Ezekiel Mudele[5], Tinashe Tapera[5], Hyeyoung Jo[1], Christopher D. Golden[5]*

[1] Interdisciplinary Program in Landscape Architecture, Seoul National University, Seoul, Republic of Korea

[2] Integrated Major in Smart City Global Convergence, Seoul National University, Seoul, Republic of Korea

[3] Department of Landscape Architecture and Rural Systems Engineering, Seoul National University, Seoul, Republic of Korea

[4] SNU Energy Initiatives, Seoul National University, Seoul, Republic of Korea

[5] Department of Nutrition, Harvard TH Chan School of Public Health, Boston, Massachusetts, United States of America

Correspondence to: Youngryel Ryu (yryu@snu.ac.kr) and Christopher D. Golden (golden@hsph.harvard.edu)

https://doi.org/10.5194/essd-2026-518
Preprint. Discussion started: 23 July 2026

Abstract

Reliable information on rice paddy cultivation is essential for food security planning in Madagascar, where rice accounts for more than half of the national caloric intake. However, the scarcity of ground reference data, high prevalence of small cropping areas, and the heterogeneity of agroecological zones have limited the production of high-resolution annual rice paddy maps across the country. Here, we present the first country-wide, annual rice paddy maps of Madagascar at 10 m resolution from 2017 to 2025. Our framework integrates three components: (1) phenology-based pseudo-label generation from 30 m merged Harmonized Landsat Sentinel-2 (HLS) time series, exploiting the flooding-to-greenup signal characteristic of transplanted rice paddy; (2) 10 m two-stage Random Forest classification on Google Satellite Embedding (GSE) annual features, refined through targeted augmentation with a small set of manually labeled samples from low-confidence regions; and (3) harmonic NDVI fitting to characterize annual cropping intensity. The pseudo-labels formed compact and clearly separated clusters in the GSE feature space across all nine years, and only five GSE dimensions consistently contributed to rice discrimination, indicating that pre-trained embeddings encoded phenologically meaningful information for rice paddy. The two-stage classifier achieved an overall accuracy (OA) of 91.2 %, a precision of 99.0 %, a recall of 83.2 %, and an F1-score of 0.904 on independent validation samples, outperforming the SAR-based benchmark product by a wide margin. Our maps indicated an increase in mapped rice paddy extent from 886,112 ha in 2017 to 1,195,766 ha in 2025 (+34.9 %), with most gains occurring along the margins of existing paddies rather than in new frontiers. This study demonstrates that combining phenology-based pseudo-labels with pre-trained satellite embeddings provides a scalable, near label-free approach for rice paddy mapping in data-scarce regions. The annual rice paddy maps are publicly available from Zenodo at https://doi.org/10.5281/zenodo.20654510 (Kwon et al., 2026).

Graphical Abstract

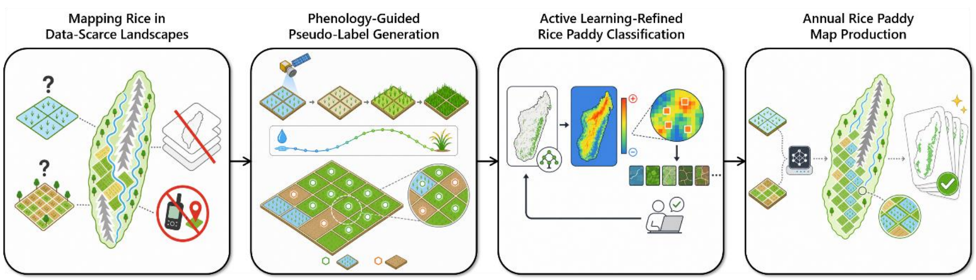

https://doi.org/10.5194/essd-2026-518
Preprint. Discussion started: 23 July 2026

Open Access Earth System Science Data Discussions

1 Introduction

Precise and timely monitoring of rice cultivation areas is essential for food security planning in countries where rice dominates both agricultural production and dietary intake (Dong and Xiao, 2016; Lobell et al., 2015). Madagascar is a clear example of this dependency, as rice accounts for approximately half of the national caloric intake, and the country ranks among the highest in per-capita rice consumption globally (Ashtakala et al., 2025; Golden et al., 2024; Nishide et al., 2026). Despite the crucial role of rice in Madagascar, few studies have produced annual rice paddy maps (Rigden et al., 2022). The lack of spatially explicit information on where, when, and how much rice is cultivated in Madagascar has limited further analyses, such as yield forecasting, irrigation planning, and food crisis early warning (Fao, 2023; Golden et al., 2025). Recent climate-related droughts and food-security crises in Madagascar have highlighted the vulnerability of rice-dependent agricultural systems, underscoring the need for annual, spatially explicit rice paddy maps to support yield forecasting, irrigation planning, and early warning (Rigden et al., 2024).

Satellite-based remote sensing has proven to be an effective tool for detecting paddy rice by exploiting the unique phenological signature of flooded conditions (Xiao et al., 2006; Zaheer et al., 2023; Zhao et al., 2024). Unlike most other crops, rice paddies often include periods of standing water during early growth stages, producing a distinctive spectral signal in which the Land Surface Water Index (LSWI) exceeds the Normalized Difference Vegetation Index (NDVI) (Xiao et al., 2005; Yang et al., 2024). This spectral signal enables phenology-based algorithms to distinguish rice from other land cover types (Dong et al., 2016; Dong et al., 2015; Ni et al., 2021). In addition, Kwon et al. (2026) demonstrate that a single gap-free LSWI−NDVI image derived from Sentinel-2 archives can provide sufficient information to detect rice paddy in smallholder landscapes.

However, the lack of ground reference data remains a central bottleneck for rice paddy detection in developing countries (Yan and Ryu, 2021; Kwon et al., 2026; Tang et al., 2026). Although there have been attempts to employ crowdsourced ground references to produce rice paddy maps in Madagascar, spatially and temporally biased samples can substantially constrain mapping accuracy in countries with heterogeneous landscapes (De Vos et al., 2023). In this context, pseudo-labeling methods, which generate training samples from physically interpretable satellite signals rather than human annotation, enable near label-free mapping in data-scarce regions (You et al., 2023; Yang et al., 2021). For example, recent studies have demonstrated the feasibility of detecting rice paddy across Africa without extensive ground references (Jiang et al., 2024). Nevertheless, the reliability of pseudo-labels has not been rigorously evaluated at the country scale, particularly in ecologically heterogeneous environments such

https://doi.org/10.5194/essd-2026-518
Preprint. Discussion started: 23 July 2026

as Madagascar.

The recent emergence of pre-trained satellite embeddings offers a new opportunity for rice paddy mapping, as they achieve higher accuracy than traditional mapping methods while requiring fewer labeled samples (Fang et al., 2026). Google Satellite Embedding (GSE) is a representative example of a global, analysis-ready dataset of learned geospatial embeddings (Brown et al., 2025; Gorelick et al., 2017). GSE compresses various Earth observation datasets into compact 64-dimensional annual feature vectors at 10 m resolution, capturing spectral and temporal patterns without requiring hand-crafted feature engineering (Brown et al., 2025). These embeddings have therefore shown strong performance in general land cover classification (Mantey et al., 2025; Li and Yu, 2025). Yet, their potential for crop type mapping, particularly for rice paddy, has not been systematically evaluated. Integrating pseudo-labels derived from phenological rules with GSE-based classification could yield a fully automated, near label-free rice mapping framework applicable wherever both data sources are available.

In this study, we present the first annual, country-wide rice paddy maps of Madagascar at 10 m resolution, covering nine consecutive years (2017–2025), produced without costly field campaigns. Our framework integrates three components to address the challenges. First, we generated pseudo-labels from optical satellite-derived phenological indicators, using the LSWI–NDVI flooding signal to identify rice paddy without relying on extensive ground reference data. Second, we classified GSE annual embeddings using these pseudo-labels, and then refined the classifier through targeted augmentation with a small number of manually labeled samples from low-confidence regions, where fragmented fields, mixed pixels, or spectrally similar land cover types can reduce classification reliability. Third, we applied harmonic NDVI fitting to characterize cropping intensity over the mapped rice paddy areas. Finally, we used the resulting maps to characterize the changing cultivation dynamics of rice paddy across Madagascar.

2 Materials and methods

2.1 Study Area

Madagascar is the fourth-largest island in the world, located in the western Indian Ocean off the southeastern coast of Africa (Fig. 1). The island spans diverse agroecological zones, ranging from humid tropical lowlands along the eastern coast to semi-arid regions in the south and west, with a central highland plateau exceeding 1,000 m in elevation, and a maximum altitude of 2,876 m (Fig. 1d and Fig. 1e). Although Madagascar's official regional structure changed during the study period, all regional analyses in this study used a fixed 22-region administrative boundary for temporal consistency. Rice is

https://doi.org/10.5194/essd-2026-518
Preprint. Discussion started: 23 July 2026

cultivated across nearly all 22 administrative regions, with production concentrated in the western lowlands (Betsiboka, Boeny, Menabe), the Lac Alaotra basin (Alaotra-Mangoro), and central highland valleys (Fig. 1a) (Rigden et al., 2022). The rice cropping calendar follows the southern hemisphere wet season, with the main growing season from November to April, while irrigated areas in some regions support a second cropping season (Ge et al., 2025). This study focuses on rice paddy systems (Fig. 1b), which dominate rice cultivation in Madagascar and exhibit detectable flooding-related phenological signals. Other minor rice systems, including swidden, direct-seeded, and intercropped rice, were not considered because they lack these characteristic spectral dynamics.

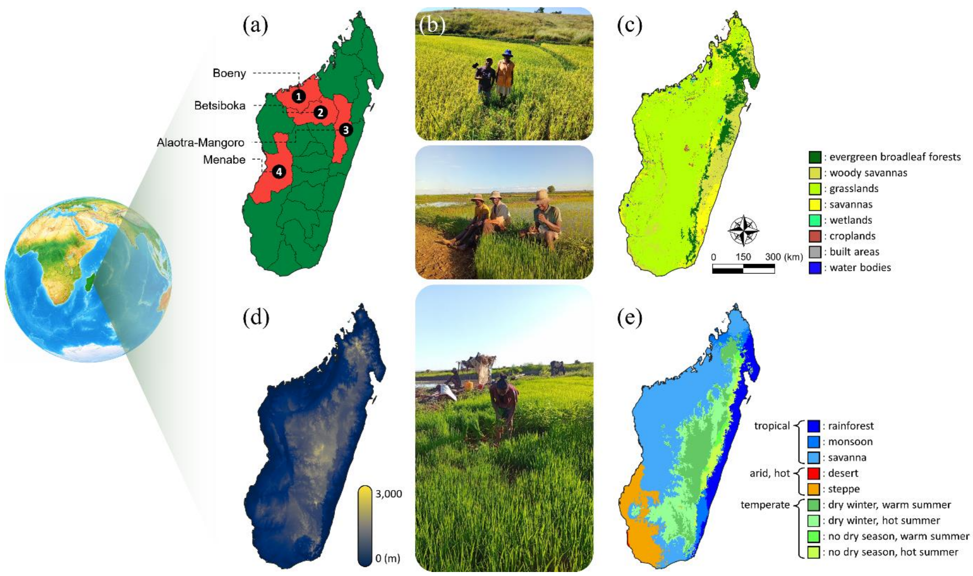

Figure 1. Study area and environmental setting of Madagascar. (a) Administrative regions, with major rice-producing regions highlighted. (b) Field photographs of rice paddies from major rice-growing regions. (c) Land cover from the MCD12Q1.061 MODIS Land Cover Type Yearly products. (d) Elevation from the Shuttle Radar Topography Mission. (e) Köppen climate zones (Peel et al., 2007).

2.2 Overall Framework

Our label-free rice paddy mapping framework consists of five sequential components: (1) land cover classification using GSE embeddings to isolate cropland and flooded vegetation, (2) rice phenology analysis from HLS-derived spectral indices to characterize the flooding-to-greenup signal, (3) rule-based pseudo-label generation from high-confidence phenological conditions, (4) rice paddy detection through two-stage Random Forest classification on GSE embeddings, and (5) cropping intensity

https://doi.org/10.5194/essd-2026-518
Preprint. Discussion started: 23 July 2026

estimation via harmonic NDVI fitting (Fig. 2). The rationale for separating pseudo-label generation (HLS, 30 m) from classification (GSE, 10 m) is that HLS provides the dense temporal observations needed to detect rice-specific phenological signals, while GSE provides higher spatial resolution and gap-free annual features for wall-to-wall mapping. Because phenology-based pseudo-labels are designed to capture clear rice signals rather than all ambiguous cases, the second classification stage used a small set of targeted hard samples, defined here as manually interpreted samples from low-confidence or error-prone pixels, to refine predictions in low-confidence areas.

https://doi.org/10.5194/essd-2026-518
Preprint. Discussion started: 23 July 2026

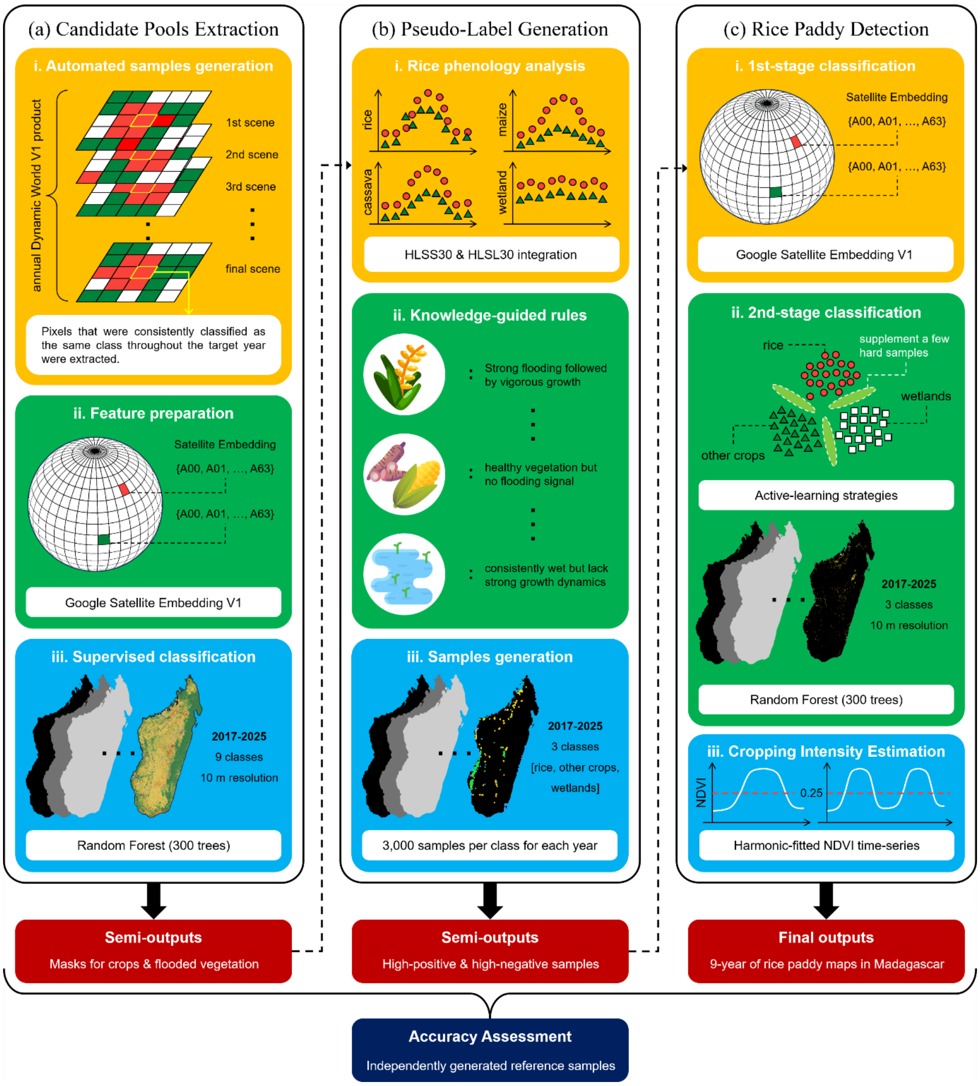

Figure 2. Overall framework for annual rice paddy mapping in Madagascar from 2017 to 2025. The workflow consists of three components: (a) land cover classification using stable annual samples derived from the Dynamic World product and Google Satellite Embedding (GSE) features, (b) pseudo-label generation using merged Harmonized Landsat Sentinel-2 (HLS) time series and knowledge-guided phenological rules, and (c) rice paddy detection and cropping intensity estimation. Accuracy assessment was conducted using independently generated reference samples.

https://doi.org/10.5194/essd-2026-518
Preprint. Discussion started: 23 July 2026

2.3 Datasets

2.3.1 Google Satellite Embedding V1 (GSE)

We used the Google Satellite Embedding V1 annual dataset available through Google Earth Engine (GEE). GSE is a global, analysis-ready dataset of learned geospatial embeddings at 10 m spatial resolution, where each pixel is represented by a 64-dimensional annual feature vector (Brown et al., 2025; Gorelick et al., 2017). These embeddings are derived by compressing multi-source Earth observation data into compact representations that capture spectral, temporal, and spatial patterns through a pre-trained neural network. Each pixel is described by embedding dimensions A00 through A63, which do not correspond to individual spectral bands but instead encode latent features learned from large-scale satellite data. Because these features integrate information across time and sensors, they provide gap-free annual representations without the need for hand-crafted feature engineering (Brown et al., 2025). In this study, GSE embeddings were used as the sole input features for both land cover classification (Section 2.4.1) and rice paddy detection (Section 2.4.4).

2.3.2 Harmonized Landsat Sentinel-2 (HLS)

We used the Harmonized Landsat Sentinel-2 (HLS) Version 2 product for phenological analysis and pseudo-label generation. To maximize temporal density, we merged the Sentinel-2–derived surface reflectance (HLSS30) and Landsat-8/9–derived surface reflectance (HLSL30) collections. Both products provide a spatial resolution of 30 m, and their combined use substantially increases observation frequency while improving the availability of dense time-series data. This high temporal resolution is particularly important for pseudo-label generation because the flooding signal of rice paddy, characterized by temporarily higher LSWI than NDVI during the short transplanting or early inundation period, often persists only for a limited time. Cloud and cloud-shadow pixels were removed using the Fmask quality band. From the cloud-free observations, we computed two spectral indices:

$$NDVI = \frac{NIR - Red}{NIR + Red} \qquad \text{(Eq. 1)}$$

$$LSWI = \frac{NIR - SWIR1}{NIR + SWIR1} \qquad \text{(Eq. 2)}$$

where *NIR* and *Red* denote the near-infrared and red bands, respectively. For LSWI, *SWIR1* refers to the shortwave infrared band. NDVI captures vegetation vigor and photosynthetic activity (Tucker, 1979), while LSWI is sensitive to surface and canopy water content (Gao, 1996).

https://doi.org/10.5194/essd-2026-518
Preprint. Discussion started: 23 July 2026

We selected these indices for two main reasons. First, NDVI effectively captures crop growth dynamics and seasonal vegetation cycles (Pettorelli et al., 2005). Second, LSWI is particularly effective for detecting surface water and identifying irrigation signals associated with rice paddy during early growth stages (Xiao et al., 2005). Together, these indices provide a physically interpretable basis for distinguishing rice paddies from other land cover types based on their characteristic flooding-to-greenup phenology (Ajadi et al., 2021; Xiao et al., 2005).

2.3.3 Dynamic World V1

We used the Dynamic World V1 product to generate reference samples for land cover classification (Brown et al., 2022). Dynamic World provides per-scene land cover classifications at 10 m resolution across nine classes, including water, trees, grass, flooded vegetation, crops, shrub and scrub, built areas, bare ground, and snow or ice. We selected Dynamic World because it offers a combination of high spatial resolution, global coverage, and continuous multi-year availability. Unlike most publicly available land cover products that provide only annual or static maps at coarser resolution, Dynamic World generates classifications for individual Sentinel-2 scenes, enabling temporally detailed land cover information throughout each year. This scene-level frequency is particularly effective for constructing annual stable training samples that represent recent land surface conditions. In addition, its global and publicly accessible framework enhances methodological reproducibility and facilitates transferability of the workflow to other regions and years.

2.3.4 Validation Datasets

We evaluated the land cover classification and rice paddy detection results using independently generated reference samples. All reference data were manually interpreted from high-resolution Sentinel-2 RGB imagery, supplemented with time-series analysis of HLS-derived spectral indices. The interpretation process was further supported by local expertise in Madagascar rice systems, with one of our team members (HJR) manually validating samples to ensure reliable identification of rice paddies across diverse landscapes. For the land cover classification, reference samples were labeled based on visual interpretation of Sentinel-2 imagery, focusing on clear and homogeneous land cover patches. For rice paddy detection, the labeling process additionally incorporated annual time-series profiles of NDVI and LSWI derived from HLS data to ensure precise identification of rice-specific phenological patterns. We collected 1,000 pointwise samples for each class, distributed across diverse climatic zones in Madagascar to mitigate spatial bias.

https://doi.org/10.5194/essd-2026-518
Preprint. Discussion started: 23 July 2026

2.3.5 Benchmark rice mapping product

To compare our rice paddy maps with an existing high-resolution rice product, we used the 20 m Africa rice distribution map of 2023 (Jiang et al., 2024). This product covers 34 rice-producing African countries, including Madagascar, and was generated using multi-source Sentinel-1 SAR and Sentinel-2 optical time series data. The authors first constructed rice samples through fast coarse positioning using Sentinel-1 VH time-series features and visual interpretation with auxiliary datasets. Then, they produced the final rice map using object-based segmentation from Sentinel-2 optical features and Random Forest classification based on selected Sentinel-1 SAR features. The reported average validation accuracy exceeded 85 %, and the mapped rice area showed strong agreement with national statistical data, with coefficients of determination above 0.9. In this study, we used this 2023 Africa rice map as the benchmark product to evaluate the relative performance of our Madagascar rice paddy mapping framework.

2.4 Methods

2.4.1 Candidate Pseudo-Labels Pools Extraction

To avoid generating pseudo-labels across irrelevant land covers such as forest, permanent water, and built areas, we produced annual land cover maps for Madagascar (Fig. 2a). For each year from 2017 to 2025 and for each administrative region, we identified stable pixels in the Dynamic World data, defined as those where the most frequent class label accounted for at least 90 % of all available observations within the year, with a minimum of five valid observations. From these stable pixels, we sampled up to 1,000 pixels per land cover class per region, resulting in a stratified reference dataset without manual labeling. We then trained a Random Forest classifier with 300 trees for each region and year using the GSE annual embeddings and the Dynamic World–derived samples. The Random Forest algorithm is an ensemble technique that produces predictions by aggregating the outputs of multiple decision trees for classification or regression tasks (Breiman, 2001).

To define the candidate pools for rice paddy mapping, we first classified all 10 m pixels into nine land cover classes following the Dynamic World scheme. We then preserved only pixels classified as cropland or flooded vegetation for subsequent rice paddy mapping. This masking step established the class structure used in the workflow. Cropland pixels were treated as potential rice paddy or other crops, while flooded vegetation pixels were treated as potential rice paddy or wetlands. We therefore targeted

https://doi.org/10.5194/essd-2026-518
Preprint. Discussion started: 23 July 2026

rice paddy, other crops, and wetlands in the pseudo-labeling and rice paddy classification steps. All remaining Dynamic World land cover classes were grouped as other land covers in the subsequent analysis.

2.4.2 Rice Phenology Analysis

To generate rice paddy pseudo-labels, we used the flooding-to-greenup phenological signal of transplanted rice paddy. During the early growth stages, standing water causes LSWI to temporarily exceed NDVI, followed by a rapid increase in vegetation greenness as the canopy develops (Fig. 3) (Xiao et al., 2005; Yang et al., 2024). We combined this LSWI–NDVI flooding signal with additional NDVI-based metrics to distinguish rice paddy from other crops and flooded wetlands.

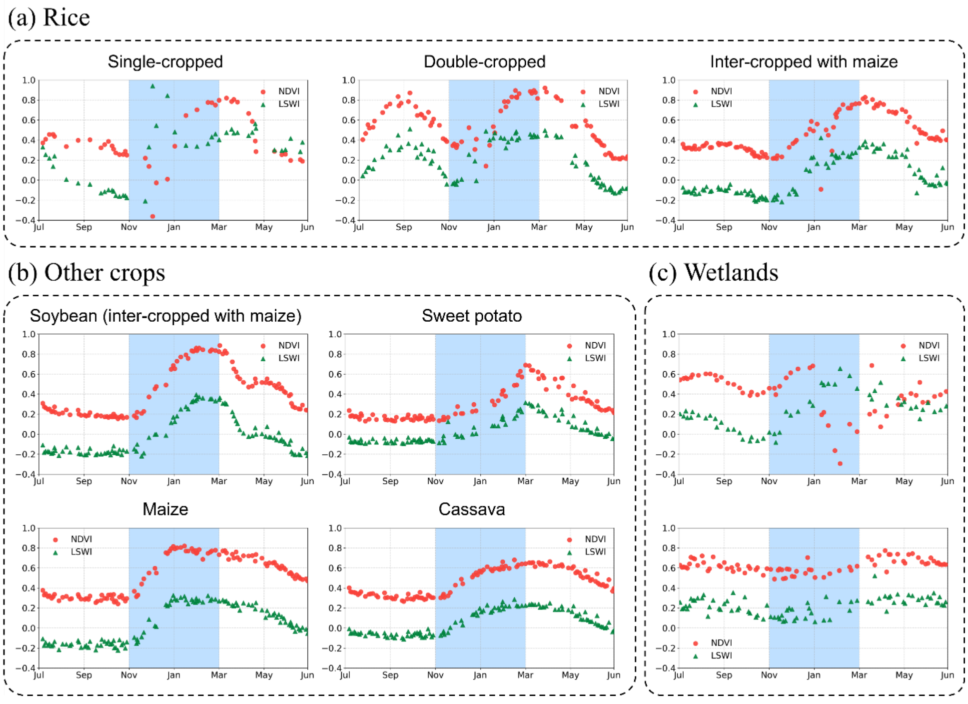

Figure 3. Representative NDVI and LSWI seasonal profiles used for rice phenology analysis in Madagascar. Examples are shown for (a) rice systems, including single-cropped, double-cropped, and rice intercropped with maize, (b) other crops, and (c) wetlands. Shaded areas indicate the early growth period when standing water is commonly present in rice paddies.

https://doi.org/10.5194/essd-2026-518
Preprint. Discussion started: 23 July 2026

Specifically, we derived a set of phenological features from the HLS time series to characterize rice growth dynamics for each year. Because Madagascar is located in the Southern Hemisphere, the annual analysis window was defined from July 1 of the preceding year to June 30 of the target year. Using the merged HLS time series, we computed six features per pixel. These included the 95th percentile of the difference between LSWI and NDVI as the primary flooding indicator, the annual maximum NDVI representing peak vegetation vigor, and the NDVI amplitude describing the strength of seasonal growth. We also calculated the number of cloud-free observations to ensure sufficient temporal coverage, along with the day of year of peak NDVI and the timing of the maximum LSWI–NDVI difference to capture flooding dynamics. These features, along with the pre-defined land cover mask, were integrated to form an eight-band feature stack at 30 m spatial resolution for each year.

2.4.3 Pseudo-Label Generation

To generate pseudo-labels within the candidate pools, we developed a knowledge-guided, rule-based approach for three classes, including rice paddy, other crops (e.g., cassava, maize, and soybean), and flooded wetlands through multiple iterative experiments (Fig. 2b). Pseudo-labeling was applied only to pixels within the cropland or flooded vegetation mask, excluding permanent water areas and pixels with incomplete phenological information. All percentile-based thresholds were calculated separately for each year within this candidate pool to account for inter-annual variability.

To assign pseudo-labels to candidate pools, we defined class-specific rules based on flooding intensity, vegetation growth, and phenological timing (Table 1). Rice pixels were identified by combining a strong flooding signal, high vegetation vigor, and a pronounced seasonal growth pattern. In addition, the timing of peak vegetation was required to occur after the flooding signal, ensuring the expected transition from inundation to canopy development. In contrast, other crop pixels were defined as actively growing cropland with moderate vegetation vigor but minimal flooding signal. Flooded wetlands were distinguished by persistent water signals combined with low seasonal variation in vegetation, separating them from rice paddies that exhibit strong growth cycles.

To ensure label consistency, we excluded any pixel that satisfied the conditions of more than one class. We then applied spatial filtering to mitigate noise by removing small isolated patches using eight-connected component analysis and retaining only pixels supported by at least three neighboring pixels of the same class within the eight-neighborhood. Each labeled pixel was assigned a confidence score ranging from 0 to 1 based on its phenological characteristics. For classifier training, we selected the

https://doi.org/10.5194/essd-2026-518
Preprint. Discussion started: 23 July 2026

Open Access Earth System Science Data Discussions

highest-confidence samples, preserving 3,000 samples per class for each year, resulting in a balanced training dataset across classes.

Table 1. Rule-based criteria used for pseudo-label generation of rice, other crops, and wetlands. Class labels were assigned using percentile-based thresholds derived annually from candidate pools based on phenological indicators related to flooding intensity, vegetation growth, and seasonal dynamics. Percentiles (p10, p25, p50, p60, p75, and p95) were calculated separately for each year to account for inter-annual variability.

Class	Condition	Description
Rice	Number of cloud-free observations ≥ p60	Sufficient temporal coverage
	Annual maximum NDVI ≥ p75	High vegetation vigor
	NDVI temporal variability ≥ p75	Strong seasonal growth cycle
	95th percentile of (LSWI − NDVI) ≥ p95	Strong flooding signal
	Day of year of maximum NDVI > day of year of maximum (LSWI − NDVI)	Flooding precedes peak greenness
Other crops	Number of cloud-free observations ≥ p60	Sufficient temporal coverage
	Annual maximum NDVI ≥ p50	Moderate vegetation vigor
	NDVI temporal variability ≥ p50	Moderate seasonal growth
	95th percentile of (LSWI − NDVI) ≤ p10	Minimal flooding signal
Wetlands	Number of cloud-free observations ≥ p60	Sufficient temporal coverage
	Annual maximum NDVI ≤ p75	Limited vegetation growth
	NDVI temporal variability ≤ p25 **or** day of year of maximum NDVI < day of year of maximum (LSWI − NDVI)	Weak seasonal variation or peak greenness preceding flooding

2.4.4 Rice Paddy Detection

To improve the accuracy of the rice paddy detection, we implemented a two-stage classification framework (Fig. 2c). In the first stage, we trained a Random Forest classifier with 300 trees using the GSE annual embeddings as input features and the pseudo-labels as training data. The classifier distinguished three classes, including rice, other crops, and flooded wetlands. We performed model training and prediction at the country scale for each year, and we compiled the classification results to produce annual rice paddy maps. The outputs were masked to preserve only pixels within the cropland and flooded vegetation areas. The classifier also provided per-pixel class probabilities, which were used to assess prediction confidence, and feature importance values were extracted to identify the most relevant embedding dimensions for rice paddy detection.

After the first-stage classification, we used the resulting confidence maps to identify areas where

https://doi.org/10.5194/essd-2026-518
Preprint. Discussion started: 23 July 2026

phenology-based pseudo-labels were less sufficient, including fragmented field boundaries, wetland margins, and spectrally mixed cropland. We then applied a second-stage refinement through targeted hard-sample augmentation. Visual inspection of the initial maps revealed systematic errors concentrated in low-confidence regions, including confusion between rice and wetlands and misclassification of non-cropland areas (Fig. S1). To address these errors, we selected uncertain pixels from the confidence maps and manually labeled a small number of hard samples using high-resolution imagery and time-series analysis of NDVI and LSWI. These hard samples represented difficult decision cases, including fragmented field boundaries, wetland margins, mixed cropland, and spectrally similar non-rice areas. They were combined with the predefined pseudo-labels by adding 1,000 hard samples per class per year from low-confidence regions. A Random Forest classifier with 300 trees was then retrained using the expanded training set and applied countrywide for each year.

2.4.5 Cropping Intensity Estimation

To estimate cropping intensity, defined as the number of rice cropping cycles per year within each detected rice paddy pixel, we analyzed seasonal NDVI dynamics using harmonic regression (Fig. 2c). For each year, we constructed cloud-free HLS NDVI time series by merging Sentinel-2 and Landsat observations within the defined growing season window. We then fitted a second-order harmonic regression model with two Fourier terms to the NDVI time series for each rice pixel:

$$NDVI(t) = a_0 + a_1 t + \sum_{k=1}^{2} [b_k \cos(2\pi kt) + c_k \sin(2\pi kt)] \qquad \text{(Eq. 3)}$$

where *t* represents time in fractional years since the start of the growing season. The fitted model was evaluated at daily intervals to generate a smoothed NDVI trajectory.

We then counted local maxima in the fitted NDVI curve to determine the cropping intensity. A valid peak was defined as a point where NDVI exceeded both the preceding and following daily values and reached a minimum value of 0.25. The number of peaks was limited to a maximum of two, as triple cropping is rare in Madagascar. Pixels with one peak were classified as single cropping, while those with two peaks were classified as double cropping. The resulting cropping intensity maps were then masked using the second-stage rice paddy detection results.

https://doi.org/10.5194/essd-2026-518
Preprint. Discussion started: 23 July 2026

2.5 Accuracy Assessment

To evaluate classification performance, we compared the predicted maps with the reference samples described in Section 2.3.4. For each year from 2017 to 2025, the classified maps were overlaid with the validation samples, and standard accuracy metrics were computed for the rice class, including overall accuracy, precision, recall, and F1-score. Overall accuracy (OA) was calculated as the proportion of correctly classified samples among all validation samples. Precision represents the fraction of predicted rice pixels that are true rice, while recall indicates the fraction of reference rice samples correctly identified by the classification. The F1-score was used to summarize the balance between precision and recall. These metrics were defined as follows:

$$OA = \frac{TP + TN}{TP + TN + FP + FN} \quad \text{(Eq. 4)}$$

$$Precision = \frac{TP}{TP + FP} \quad \text{(Eq. 5)}$$

$$Recall = \frac{TP}{TP + FN} \quad \text{(Eq. 6)}$$

$$F1 - score = \frac{2 \times (Precision \times Recall)}{Precision + Recall} \quad \text{(Eq. 7)}$$

where *TP*, *TN*, *FP*, and *FN* denote true positives, true negatives, false positives, and false negatives, respectively.

3 Results

3.1 Accuracy assessment of rice paddy classification

The detected rice paddy areas showed strong visual agreement with field-scale patterns observed in Sentinel-2 RGB imagery across ten representative sites in Madagascar (Fig. 4). These sites cover major rice-producing regions and a range of agroecological settings, including western lowland plains, central highland valleys, and eastern floodplains. The classification captured diverse paddy configurations, such as irrigated clusters on floodplains, fragmented plots along riparian corridors, and smallholder paddies embedded within mixed cropland mosaics. At the 10 m spatial resolution, paddy boundaries were generally well delineated, while adjacent land-cover types such as roads, bare soil, forest edges, and urban areas were largely excluded from the rice paddy class.

https://doi.org/10.5194/essd-2026-518
Preprint. Discussion started: 23 July 2026

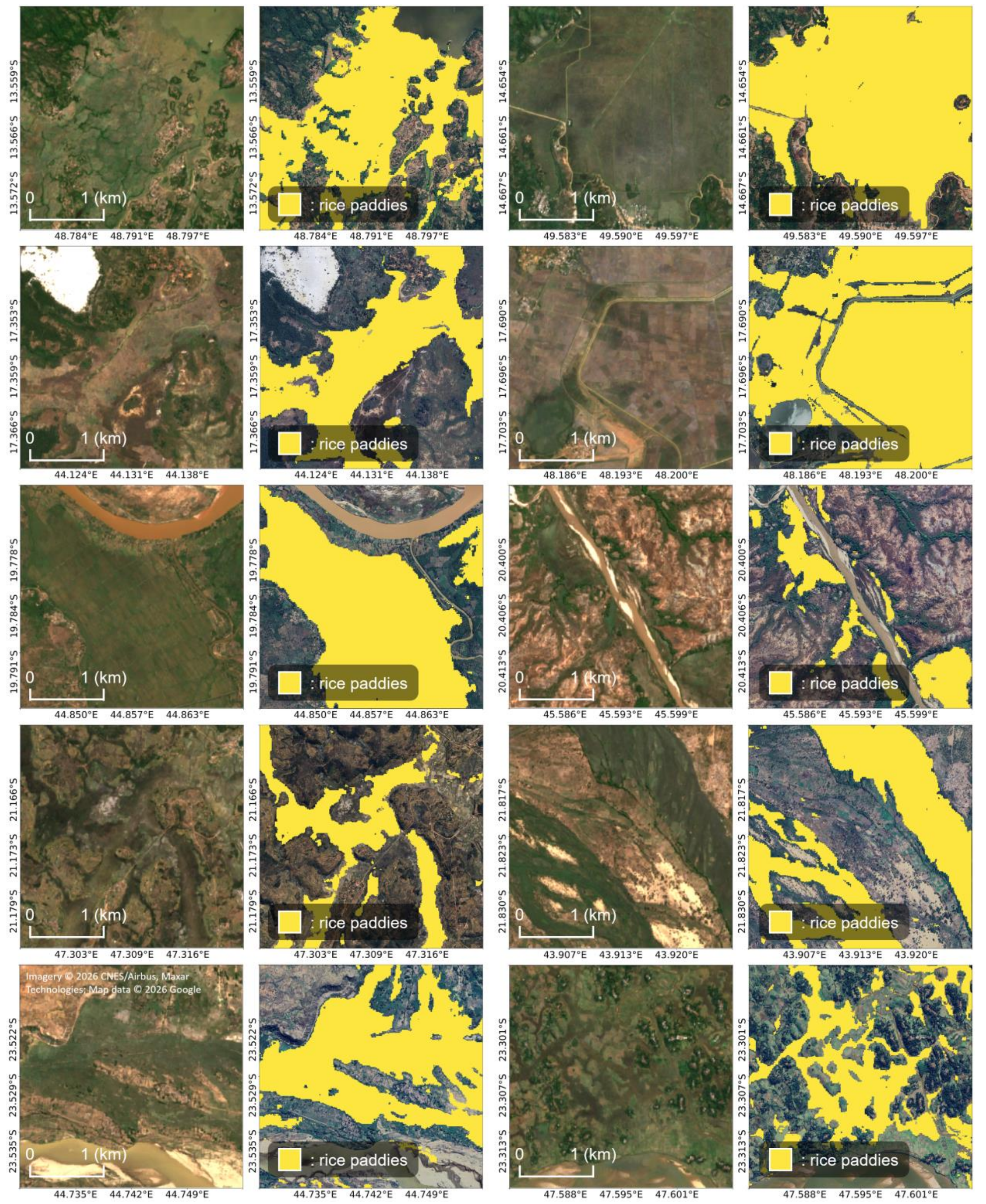

Figure 4. Zoomed-in visualizations of the rice paddy detection result across diverse locations in Madagascar. Sentinel-2 RGB imagery (left in each pair) is shown alongside the corresponding mapped rice paddies (background imagery: Imagery © 2026 CNES/Airbus, Maxar Technologies; Map data © 2026 Google).

https://doi.org/10.5194/essd-2026-518
Preprint. Discussion started: 23 July 2026

The two-stage framework outperformed the benchmark product on the same validation samples (Fig. S5). The final 2nd-stage classification achieved an OA of 91.2 %, precision of 99.0 %, recall of 83.2 %, and F1-score of 0.904, compared with 54.7 %, 66.3 %, 19.3 %, and 0.299 for the benchmark product and 76.8 %, 88.2 %, 61.9 %, and 0.728 for the 1st-stage classification, respectively (Fig. 5a). Error counts showed that the benchmark primarily suffered from omission errors, missing 808 of the 1,001 rice points, while also misclassifying 98 non-rice points as rice. In contrast, the 2nd-stage classification missed 168 rice points and produced only 8 false rice predictions. Across Köppen–Geiger climate zones, F1-scores ranged from 0.84 in the rainforest zone to 0.96 in the steppe zone, with precision remaining at or above 0.98 in all zones (Fig. 5b). Performance was highest on slopes below 5° (F1-score > 0.91), but declined on slopes of 5–10° and >10°, where F1-scores were 0.73 and 0.46, respectively. These steeper slope classes accounted for only 4.7 % and 0.4 % of mapped rice paddy pixels, respectively (Table S1 and Fig. S2).

https://doi.org/10.5194/essd-2026-518
Preprint. Discussion started: 23 July 2026

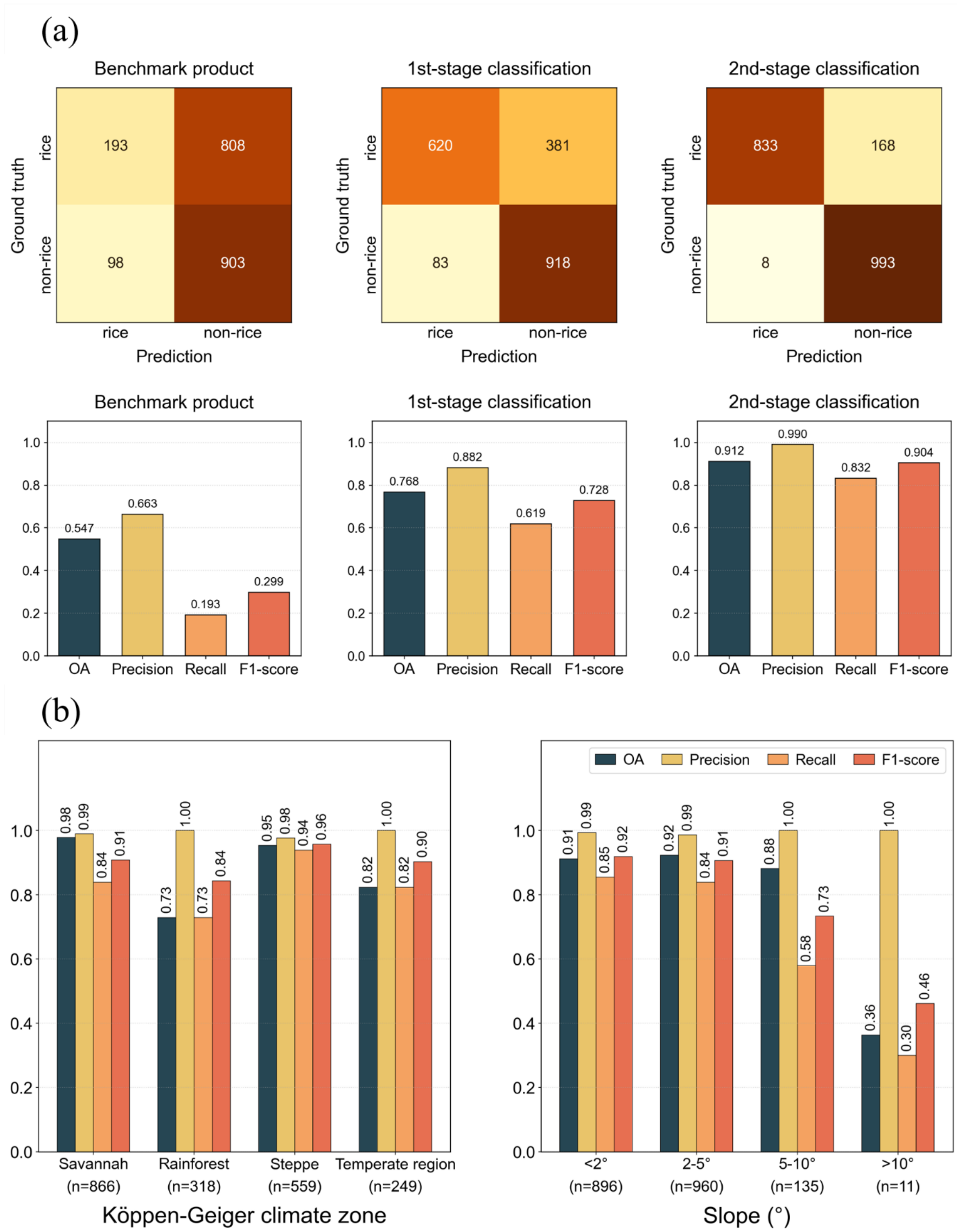

Figure 5. Accuracy evaluation of the rice paddy maps against ground-truth validation points. (a) Confusion matrices (top) and metric bars (bottom) for the benchmark product, the 1st-stage classification on the candidate pools, and the final 2nd-stage classification. (b) Stratified accuracy of the 2nd-stage classification by Köppen-Geiger climate zone (left) and slope class (right). OA denotes overall accuracy.

https://doi.org/10.5194/essd-2026-518
Preprint. Discussion started: 23 July 2026

3.2 Pseudo-label separability in the GSE embedding space

Pseudo-labeled samples of rice paddies, other crops, and flooded wetlands formed largely distinct clusters in the GSE feature space across all target years (Fig. 6). The t-distributed stochastic neighbor embedding (t-SNE) projections of the 64-dimensional annual GSE embeddings showed clear grouping by class, with limited overlap among the three pseudo-label categories. Rice paddy samples formed a relatively compact cluster throughout the nine-year period, whereas flooded wetlands occupied a separate region of the embedding space. In some years, particularly 2020 and 2021, wetlands showed partial overlap with other crops, but they remained well separated from rice paddies. This consistent class separation suggests that the pseudo-labels captured meaningful patterns in the GSE features that were broadly stable across years.

https://doi.org/10.5194/essd-2026-518
Preprint. Discussion started: 23 July 2026

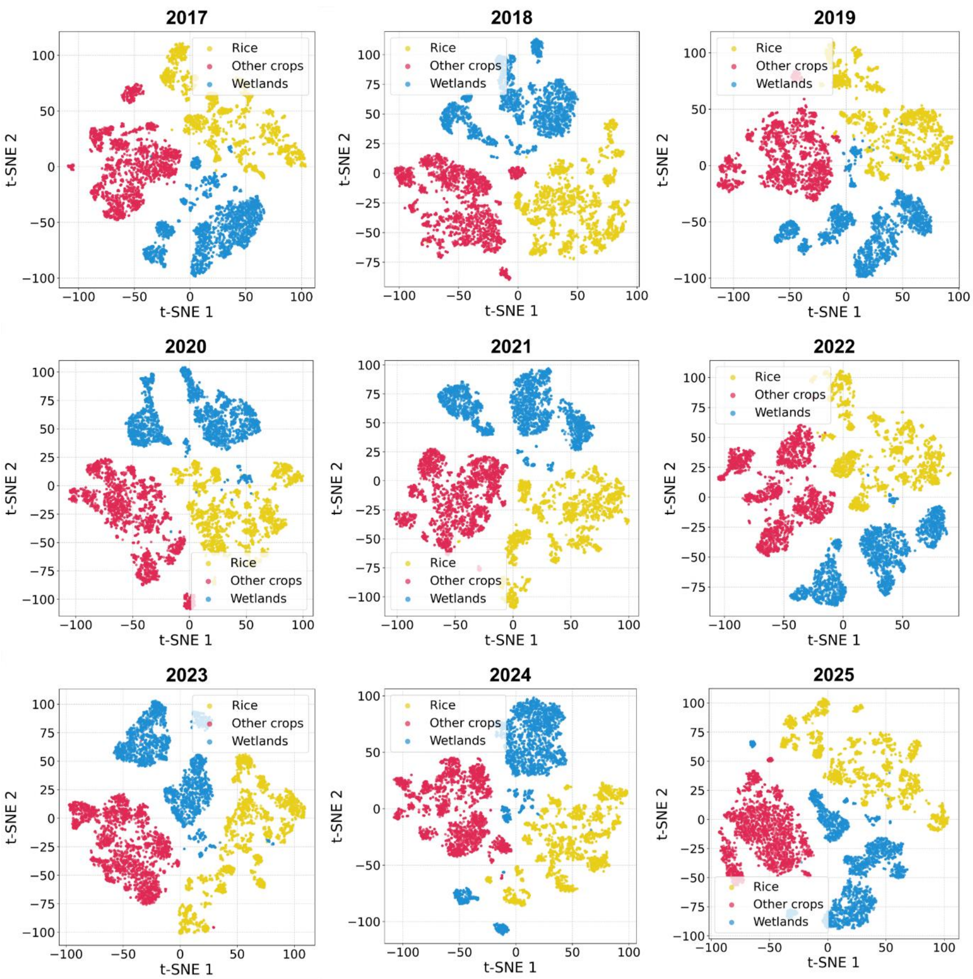

Figure 6. t-SNE visualization of pseudo-label feature separability for rice, other crops, and wetlands from 2017 to 2025. Each panel represents one year, showing the clustering patterns of samples in the embedded feature space.

Five GSE embedding dimensions, A38, A20, A19, A51, and A09, consistently ranked among the most important features for rice paddy classification from 2017 to 2025 (Fig. 7). Among these, A38 had the highest normalized importance in seven of the nine years, reaching approximately 4 %. The other four dimensions remained within the top 15 features in all years and within the top five in most years. This temporal consistency suggests that a small subset of GSE dimensions contributed reliably to rice paddy discrimination, despite year-to-year variation in phenology and cloud conditions. By contrast, most of

https://doi.org/10.5194/essd-2026-518
Preprint. Discussion started: 23 July 2026

the remaining 59 dimensions contributed less than 2 % in each year and showed greater variation in their rankings over time.

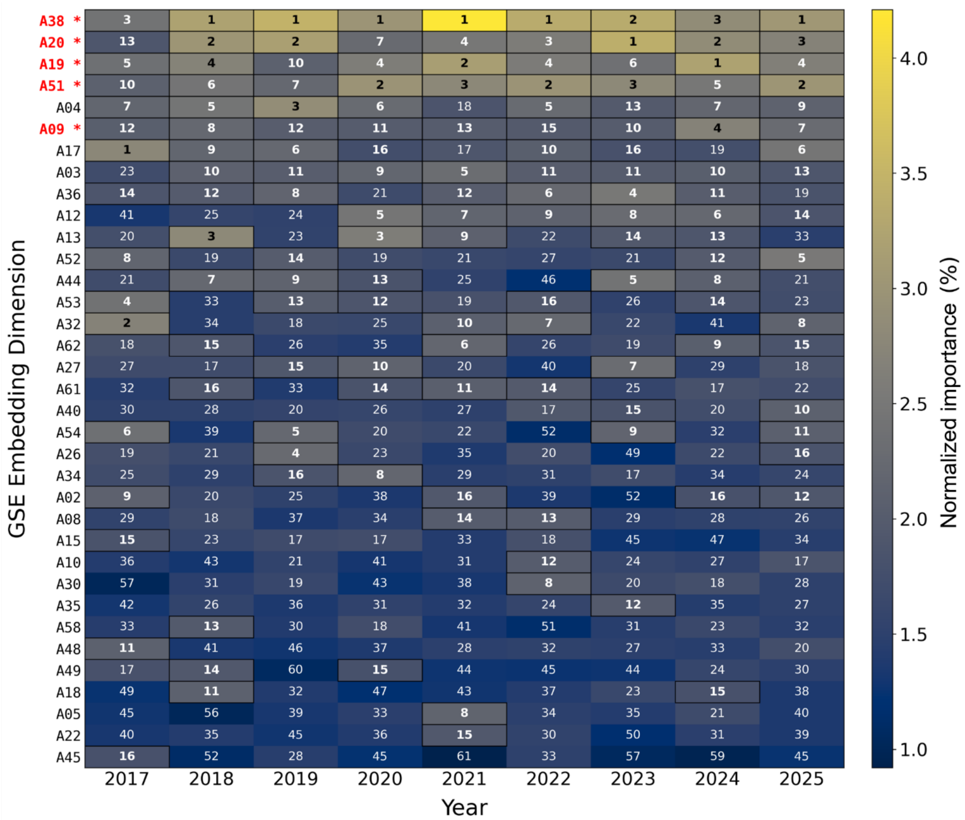

Figure 7. Normalized feature importance of GSE embedding dimensions for rice paddy classification from 2017 to 2025. Each row represents a GSE feature (A00–A63), and columns correspond to individual years. Values indicate normalized importance (%) derived from the Random Forest model, with features ordered by overall importance ranking. Consistent high-importance features across years highlight stable embedding dimensions contributing to rice discrimination.

3.3 Changes in annual rice paddy area across Madagascar, 2017 to 2025

The mapped extent of rice paddy across Madagascar increased in our annual maps from 886,112 ha in 2017 to 1,195,766 ha in 2025, representing a net gain in mapped paddy extent of approximately 309,655 ha (+34.9 %), over the nine-year period (Fig. 8a). This increase reflected larger gains into the rice paddy class than losses from the 2017 rice paddy class. Total losses amounted to 194,630 ha, including 137,046

https://doi.org/10.5194/essd-2026-518
Preprint. Discussion started: 23 July 2026

ha converted to other land covers, 30,264 ha to other crops, and 27,320 ha to wetlands. By comparison, gains totaled 504,284 ha, consisting of 361,069 ha converted from other land covers, 74,986 ha from other crops, and 68,229 ha from wetlands. Despite a sharp decline in mapped rice paddy area in 2020, the fitted linear trend remained positive, with an average increase of 32,842 ha yr^{-1} from 2017 to 2025 (Fig. 8b).

Rice paddies were concentrated in a small number of administrative regions throughout the study period (Fig. 8c). In 2025, Boeny contained the largest mapped rice paddy area, followed by Alaotra-Mangoro, Sofia, and Menabe. Most of the five largest rice-producing regions were located in tropical savannah climate zones, whereas Alaotra-Mangoro was located in the central highlands, where the climate is classified as temperate with a dry winter and hot summer. The smallest mapped rice paddy areas were observed in Androy and other southern arid regions, each with less than 1×10^4 ha. The annual transition patterns further showed that rice paddy classification was not fixed at the pixel level (Fig. 8d). Among pixels mapped as rice paddy in both 2017 and 2025, 45.3 % were classified as non-rice in at least one intervening year. Similarly, among pixels mapped as rice paddy in 2017 but not in 2025, 79.0 % returned to the rice paddy class at least once during the study period.

https://doi.org/10.5194/essd-2026-518
Preprint. Discussion started: 23 July 2026

Open Access Earth System Science Data Discussions

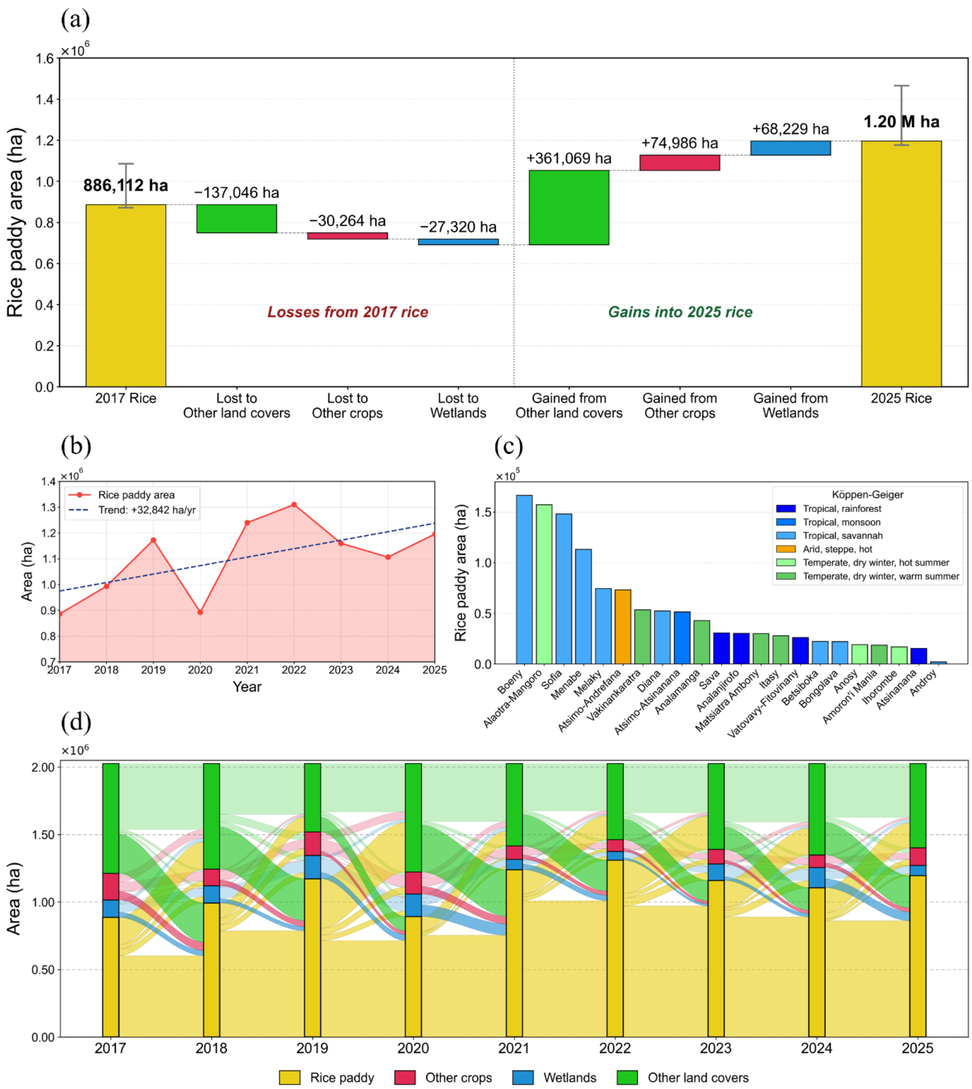

416

417 **Figure 8.** Temporal changes in the rice paddy area in Madagascar from 2017 to 2025. (a) Net rice paddy gains and losses by land cover transition, (b) annual rice paddy area and linear trend, (c) 2025 rice paddy area by administrative region, colored by major Köppen-Geiger climate zone (Peel et al., 2007), and (d) annual land cover trajectories of all pixels mapped as rice paddy in at least one year between 2017 and 2025. Error bars on the 2017 and 2025 bars in (a) show asymmetric classification-error ranges propagated from the 2nd-stage validation results.

422

https://doi.org/10.5194/essd-2026-518
Preprint. Discussion started: 23 July 2026

Open Access Earth System Science Data Discussions

In both 2017 and 2025, rice paddies were mainly distributed across the western coastal lowlands and the north-central highlands, with smaller mapped areas in the southern dry regions and along much of the eastern coast (Fig. 9a and b). The four detailed sites showed local patterns that were consistent with the national increase in mapped rice paddy area (Fig. 9c). At all sites, gains exceeded losses between 2017 and 2025. Stable rice paddies generally formed the core paddy areas, whereas newly mapped paddies were concentrated along the margins of 2017 paddies or in nearby non-paddy areas. Losses were comparatively limited across the sites. This pattern of local expansion was consistent with the national transition results in Fig. 8a, where total gains into the rice paddy class (504,284 ha) were substantially larger than losses from the 2017 rice paddy class (194,630 ha).

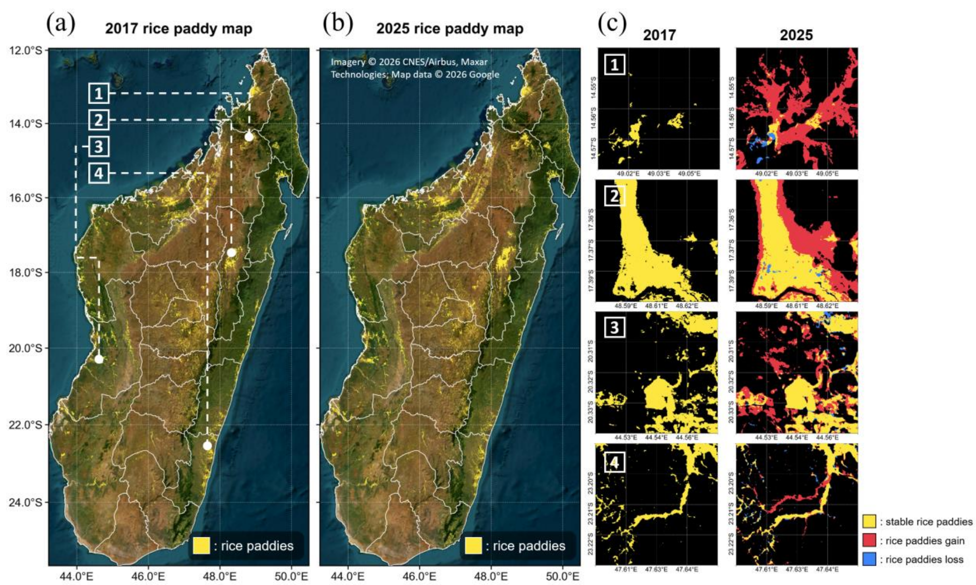

Figure 9. Spatial distribution and changes in rice paddy areas between 2017 and 2025. (a) Rice paddy distribution in 2017, (b) rice paddy distribution in 2025 (background imagery: Imagery © 2026 CNES/Airbus, Maxar Technologies; Map data © 2026 Google), and (c) zoomed-in comparisons exhibiting stable rice paddies, gains, and losses across representative regions between 2017 and 2025.

3.4 Regional rice paddy density and cropping intensity

Rice paddy density and cropping intensity showed clear regional variation across Madagascar in 2025 (Fig. 10). Rice paddy density refers to the mapped rice paddy area within each region divided by the total land area of that region, and therefore represents regional spatial concentration rather than individual plot size. Rice paddies were concentrated mainly in the western lowlands and central

https://doi.org/10.5194/essd-2026-518
Preprint. Discussion started: 23 July 2026

highlands, with additional smaller and more linear concentrations along parts of the eastern coast and lower densities in the southern dry areas (Fig. 10a). The highest rice paddy densities occurred in Alaotra-Mangoro (5.8 ha km^{-2}), Boeny (5.6 ha km^{-2}), Itasy (4.2 ha km^{-2}), and Vakinankaratra (3.1 ha km^{-2}) (Fig. 10b). Some regions with large mapped rice paddy areas had relatively lower density values, including Menabe (2.3 ha km^{-2}) and Atsimo-Andrefana (1.1 ha km^{-2}), indicating that rice paddies were more spatially dispersed in these regions. From 2017 to 2025, the largest increase in rice paddy density occurred in Alaotra-Mangoro (+3.6 ha km^{-2}), followed by Boeny and Sofia (Fig. 10c). Most other regions showed smaller changes, while Atsinanana showed a slight decline.

Cropping intensity also varied regionally in 2025. Double cropping was more common in the eastern regions, which are characterized by tropical rainforest climates and consistent rainfall across the year to support rain-fed agriculture, whereas single cropping dominated in the western and central regions where there is a prolonged dry season (Fig. 10d). Regional double-cropping rates ranged from 38.8 % to 88.8 % in 2025 (Fig. 10e). The highest rates were concentrated along the eastern region of Madagascar, while many western and central highland regions remained below 60 %. Between 2017 and 2025, changes in the double-cropping rate ranged from -6.9 to +15.9 % across regions (Fig. 10f). Both increases and decreases were observed, with larger increases concentrated in parts of the eastern and southeastern regions.

https://doi.org/10.5194/essd-2026-518
Preprint. Discussion started: 23 July 2026

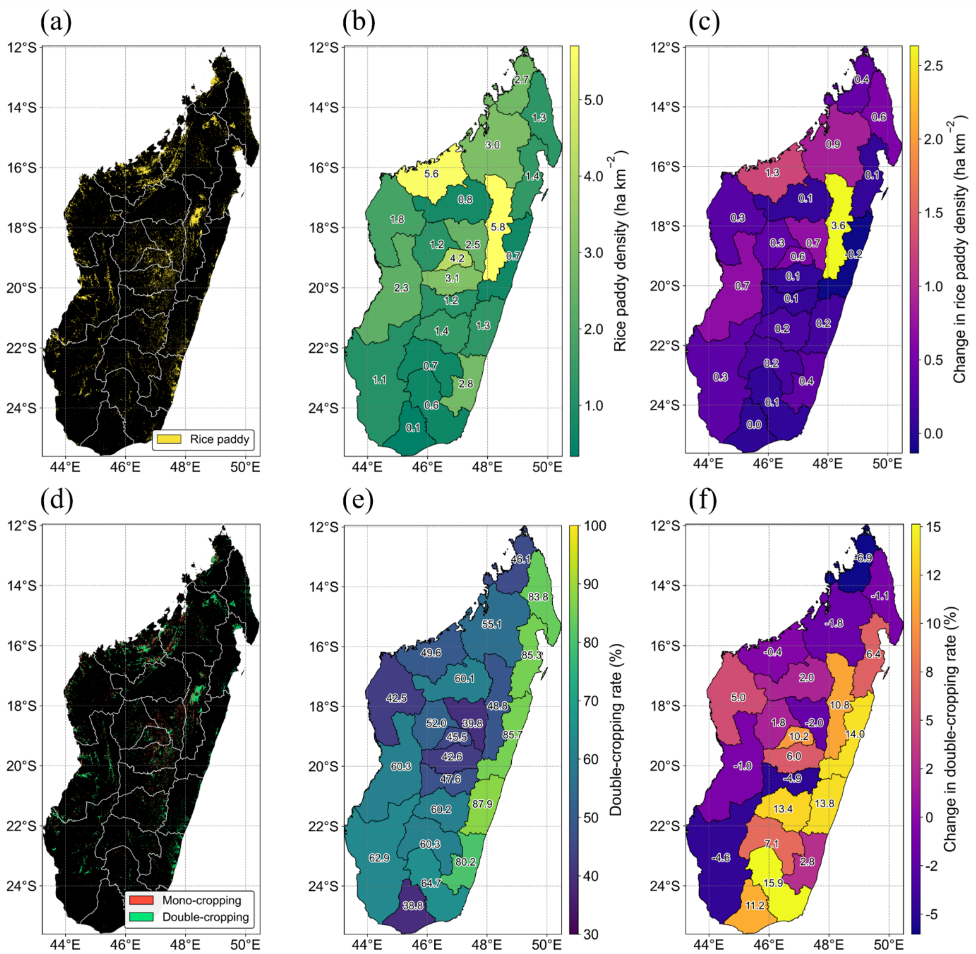

Figure 10. Spatial distribution and changes in rice paddy density and cropping intensity in Madagascar. (a) Rice paddy distribution in 2025, (b) rice paddy density, calculated as mapped rice paddy area divided by total regional land area (ha km^{-2}), by administrative region in 2025, (c) change in rice paddy density between 2017 and 2025, (d) spatial distribution of single- and double-cropping systems in 2025, (e) proportion of double-cropping by region in 2025, and (f) change in double-cropping rate between 2017 and 2025.

https://doi.org/10.5194/essd-2026-518
Preprint. Discussion started: 23 July 2026

4 Discussion

4.1 Phenology-guided pseudo-labels reduced reference bias in rice mapping

Our results show that the proposed two-stage framework produced more accurate and spatially detailed rice paddy maps than the existing SAR-based benchmark, reproducing field-scale paddy patterns across Madagascar's agroecological zones (Fig. 4 and Fig. 5a). This improvement likely reflects more representative training samples rather than greater classifier complexity. Earlier rice maps for Madagascar relied on crowdsourced reference points that were concentrated near roads and towns, which likely under-represented the small and scattered paddies found across much of the country. This type of location bias is a known limitation of crowdsourced land-cover data (De Vos et al., 2023; Comber et al., 2013; Fritz et al., 2009). By deriving pseudo-labels from the flooding-to-greenup signal of transplanted rice and sampling them nationwide, our approach reduced this bias and helped the model learn paddy patterns across diverse environments. The separated clusters of rice, other crops, and wetlands in the GSE feature space further support the improved representativeness of the training samples (Fig. 6).

The pseudo-labeling rules were effective because they described the seasonal sequence of transplanted rice rather than a single spectral condition. Annual percentile thresholds allowed the rules to adjust by year without requiring prior knowledge of local rice calendars (Fig. S3), avoiding the fixed thresholds that can limit the transferability of flooding-based methods (Dong et al., 2015; Ni et al., 2021; Kontgis et al., 2015). No individual metric fully separated rice, other crops, and wetlands (Fig. S4). Instead, the flooding signal helped distinguish rice from non-flooded crops, while seasonal NDVI change helped separate rice from persistently wet areas with limited vegetation growth. Requiring the greenness peak to follow the flooding signal matched the typical growth sequence of transplanted rice and reduced confusion with wetlands, a common challenge in optical rice mapping (Yang et al., 2024; Zhao et al., 2024).

The comparison with the SAR-based benchmark suggests that optical phenology provided a more stable rice signal in Madagascar's heterogeneous landscapes (Fig. S5). The benchmark was affected by viewing geometry, terrain shadow, and overlapping orbits, particularly in the mountainous interior (Fig. S6a). Some non-rice crops also showed seasonal backscatter changes similar to flooded paddies, contributing to commission errors (Fig. S6b). These factors likely explain why the benchmark omitted many true paddies and misclassified some non-rice fields as rice (Fig. 5a). This does not imply that SAR is unsuitable for rice mapping in general, but in this setting the optical flooding-to-greenup signal was more directly linked to the water and canopy changes of transplanted rice during early growth (Xiao et al., 2005; Xiao et al., 2006).

https://doi.org/10.5194/essd-2026-518
Preprint. Discussion started: 23 July 2026

Open Access Earth System Science Data Discussions

4.2 Pre-trained embeddings captured rice phenology in a compact feature space

The GSE embeddings contained rice-related information even though they were not designed specifically for rice mapping. A small subset of the 64 dimensions ranked as important across most years (Fig. 7), and these dimensions were correlated with the flooding and greenness metrics used in the pseudo-labeling rules (Fig. S7). Rice also occupied a relatively distinct region of the embedding space, suggesting that GSE summarized part of the phenological information needed to distinguish rice from other land covers. This reduced the need for many hand-crafted indices or full seasonal feature sets, which are often used in heterogeneous landscapes (Dong et al., 2016; Ni et al., 2021; Zhao et al., 2024). Our results therefore extend earlier applications of GSE from general land cover and cropping patterns to single-crop mapping (Li and Yu, 2025).

The embeddings were also useful where the optical flooding signal was incomplete or ambiguous. In Madagascar, transplanting often coincides with heavy cloud cover, creating gaps in the HLS time series, and flooding alone can confuse rice with wetlands. Because GSE integrates information from multiple sensors and summarizes broader spectral and temporal patterns, it provided a compact input that helped reduce reliance on cloud-gap filling and manual feature engineering.

The second-stage refinement showed that a small number of targeted labels could correct many remaining errors. The first-stage model trained only on pseudo-labels still produced errors along field edges and wetland margins (Fig. S1). Adding these hand-labeled hard samples from uncertain areas improved the final classification (Fig. 5a), indicating that many errors were concentrated in a limited set of difficult locations. This agrees with earlier studies showing that targeted samples can improve classification more efficiently than random sampling (Persello and Bruzzone, 2014; Wang et al., 2019). Together, the pseudo-labels, embeddings, and targeted refinement provide a practical workflow for crop mapping where field reference data are limited.

4.3 Rice expansion was concentrated around existing paddy systems

The annual maps suggest that rice expansion in Madagascar occurred mainly around existing paddy systems rather than through large frontier conversion. This pattern is expected for paddy rice because expansion is constrained by lowland topography, water availability, and existing irrigation or valley-bottom systems. In Madagascar, broader frontier conversion is more commonly associated with upland slash-and-burn cultivation than with new paddy development. New paddies were concentrated along the margins of stable rice-growing areas in the western coastal lowlands and the central and northern

https://doi.org/10.5194/essd-2026-518
Preprint. Discussion started: 23 July 2026

highlands (Fig. 9c), with most gains occurring near paddies already present in 2017 (Fig. S8). This pattern therefore suggests incremental expansion around existing valley-bottom and irrigation systems, including areas such as the Lac Alaotra basin and the Marovoay plain (Rigden et al., 2022), rather than a large frontier-style expansion comparable to agricultural frontiers reported in regions such as the Brazilian Cerrado and the Amazon (Potapov et al., 2022. Song et al., 2021).

Rice cultivation remained concentrated in a limited number of regions. The central highland basins and western lowlands contained the densest paddies and showed some of the largest increases in paddy density over the study period (Fig. 10a, b, and c). This regional concentration may make national rice supply sensitive to local shocks, particularly because key production areas face climate hazards such as drought in the south and west and cyclones in the east (Rigden et al., 2024). The 10 m annual maps can therefore support regional yield forecasting, irrigation planning, and risk assessment in landscapes where coarser maps often fail to resolve small fields (Jin et al., 2019; Rigden et al., 2022).

Water availability also appeared to influence cropping intensity. Double cropping was concentrated in wetter eastern regions, while single cropping dominated the drier west and central highlands (Fig. 10d). This pattern suggests that the national increase in mapped paddy area was driven mainly by spatial expansion, although local increases in double cropping indicate that intensification was concentrated where further land expansion was limited (Fig. 10f). Conversely, double cropping declined in drier regions of Madagascar that have been experiencing reductions in precipitation and soil moisture over time (Rigden et al., 2024). Mapping both paddy extent and cropping intensity is therefore important for distinguishing area expansion from more frequent cultivation.

4.4 Implications for future applications

This study shows that annual 10 m rice paddy mapping is feasible in regions where ground reference data are limited. The workflow relies on public datasets, percentile-based phenological rules, pre-trained embeddings, and a Random Forest classifier, making it relatively simple to reproduce across years. The approach may also be transferable to other rice-growing regions, as preliminary applications in other African rice areas produced patterns broadly consistent with existing products (Fig. S9). However, independent validation is still needed before applying the maps operationally in new countries (Jiang et al., 2024; Jin et al., 2019). The harmonic NDVI step further allowed the maps to describe cropping intensity (Fig. 10), which could support studies of water management, methane emissions, and climate adaptation (Golden et al., 2025).

https://doi.org/10.5194/essd-2026-518
Preprint. Discussion started: 23 July 2026

The framework also provides a basis for broader agricultural monitoring in Madagascar. Similar workflows could be developed for other staple crops, such as maize and cassava, although these crops lack a clear flooding signal and would require different phenological rules. Annual crop maps could also be combined with yield models, irrigation datasets, and climate-risk layers to identify areas where extension services, irrigation investment, or early warning may be most needed.

Two limitations should be considered. First, the rules depend on the flooding signal of transplanted rice, so rice systems without a clear flooding stage, such as swidden and direct-seeded rice, are likely underrepresented. The maps should therefore be interpreted as conservative estimates of paddy rice area rather than total rice cultivation area, particularly in eastern rainforest regions where swidden rice is common. Second, GSE currently provides annual embeddings only from 2017 onward, so the framework maps rice at yearly intervals and cannot yet detect within-season changes.

5 Conclusions

This study demonstrates a scalable approach for annual rice paddy mapping in data-scarce regions by combining phenology-guided pseudo-labels with pre-trained satellite embeddings. Rather than relying on dense field reference data, the framework uses the seasonal flooding-to-greenup sequence of transplanted rice to generate training samples and uses GSE to represent rice-related phenology in a compact feature space. Applied to Madagascar, this approach produced spatially detailed maps that reveal where rice systems are expanding, where cultivation remains concentrated, and where cropping intensity varies. Beyond Madagascar, the workflow offers a practical framework for monitoring smallholder rice systems in regions where ground data are limited but public satellite data are available. Such maps can support food security assessment, irrigation planning, climate-risk monitoring, and adaptation strategies that require timely and spatially explicit information on rice cultivation.

https://doi.org/10.5194/essd-2026-518
Preprint. Discussion started: 23 July 2026

Data availability. The annual 10 m rice paddy maps of Madagascar from 2017 to 2025 described in this manuscript are available from Zenodo at https://doi.org/10.5281/zenodo.20654510 (Kwon et al., 2026).

Supplement. The supplementary material for this article is available in the attached file.

Author contributions. Author contribution. RK: Conceptualization, Methodology, Validation, Formal analysis, Writing – original draft, Writing – review & editing, Visualization. YR: Conceptualization, Funding acquisition, Project administration, Supervision, Writing – review & editing. GDN: Conceptualization, Methodology, Validation, Writing – review & editing. HR: Methodology, Validation, Writing – review & editing. OEM: Conceptualization, Methodology, Writing – review & editing. TT: Methodology, Writing – review & editing. HJ: Methodology, Writing – review & editing. CDG: Conceptualization, Funding acquisition, Project administration, Supervision, Writing – review & editing.

Competing interest. The authors declare that they have no conflict of interest.

Acknowledgements. The authors thank the institutions and collaborators that supported this research.

Financial support. This research was supported by the Rural Development Administration of the Republic of Korea (RS-2024-00397146), the Ren Che Foundation, and the Harvard Data Science Initiative, which received support from Amazon Web Services.

References

Ajadi, O. A., Barr, J., Liang, S.-Z., Ferreira, R., Kumpatla, S. P., Patel, R., and Swatantran, A.: Large-scale crop type and crop area mapping across Brazil using synthetic aperture radar and optical imagery, Int. J. Appl. Earth Obs. Geoinf., 97, 102294, https://doi.org/10.1016/j.jag.2020.102294, 2021.

Ashtakala, V., Tan, J., Dhakhwa, T., and Zhang, Y.: Madagascar rice production: Challenges and strategies for self-sufficiency, International Monetary Fund, https://doi.org/10.5089/9798229004114.002.a003, 2025.

Breiman, L.: Random forests, Mach. Learn., 45, 5-32, https://doi.org/10.1023/A:1010933404324, 2001.

Brown, C. F., Brumby, S. P., Guzder-Williams, B., Birch, T., Hyde, S. B., Mazzariello, J., Czerwinski, W., Pasquarella, V. J., Haertel, R., and Ilyushchenko, S.: Dynamic World, near real-time global 10 m land use land cover mapping, Sci. Data, 9, 251, https://doi.org/10.1038/s41597-022-01307-4, 2022.

Brown, C. F., Kazmierski, M. R., Pasquarella, V. J., Rucklidge, W. J., Samsikova, M., Zhang, C., Shelhamer, E., Lahera, E., Wiles, O., and Ilyushchenko, S.: AlphaEarth foundations: An embedding field model for accurate and efficient global mapping from sparse label data, arXiv [preprint], https://doi.org/10.48550/arXiv.2507.22291, 2025.

Comber, A., See, L., Fritz, S., Van der Velde, M., Perger, C., and Foody, G.: Using control data to determine the reliability of volunteered geographic information about land cover, Int. J. Appl. Earth Obs. Geoinf., 23, 37-48, https://doi.org/10.1016/j.jag.2012.11.002, 2013.

De Vos, K., Campforts, B., Tits, L., Van Tricht, K., Bonte, K., Govers, G., and Jacobs, L.: Potential and limitations of crowdsourced data for high-resolution rice mapping in Madagascar: The importance of representation, Int. J. Appl. Earth Obs. Geoinf., 117, 103204, https://doi.org/10.1016/j.jag.2023.103204, 2023.

Dong, J. and Xiao, X.: Evolution of regional to global paddy rice mapping methods: A review, ISPRS J. Photogramm., 119, 214-227, https://doi.org/10.1016/j.isprsjprs.2016.05.010, 2016.

Dong, J., Xiao, X., Kou, W., Qin, Y., Zhang, G., Li, L., Jin, C., Zhou, Y., Wang, J., and Biradar, C.: Tracking the dynamics of paddy rice planting area in 1986-2010 through time series Landsat images and phenology-based algorithms, Remote Sens. Environ., 160, 99-113, https://doi.org/10.1016/j.rse.2015.01.004, 2015.

Dong, J., Xiao, X., Menarguez, M. A., Zhang, G., Qin, Y., Thau, D., Biradar, C., and Moore III, B.: Mapping paddy rice planting area in northeastern Asia with Landsat 8 images, phenology-based algorithm and Google Earth Engine, Remote Sens. Environ., 185, 142-154, https://doi.org/10.1016/j.rse.2016.02.016, 2016.

Fang, H., Liang, S., Li, W., Chen, Y., Ma, H., Xu, J., Ma, Y., He, T., Tian, F., Zhang, F., and Liang, H.: Generating an annual 30 m rice cover product for monsoon Asia (2018-2023) using harmonized Landsat and Sentinel-2 data and the NASA-IBM geospatial foundation model, Remote Sens. Environ., 335, 115256, https://doi.org/10.1016/j.rse.2026.115256, 2026.

FAO: Agricultural production statistics 2000-2022, FAO, https://doi.org/10.4060/cc9205en, 2023.

Fritz, S., McCallum, I., Schill, C., Perger, C., Grillmayer, R., Achard, F., Kraxner, F., and Obersteiner, M.: Geo-Wiki.org: The use of crowdsourcing to improve global land cover, Remote Sens., 1, 345-354, https://doi.org/10.3390/rs1030345, 2009.

Gao, B.-C.: NDWI: A normalized difference water index for remote sensing of vegetation liquid water

https://doi.org/10.5194/essd-2026-518
Preprint. Discussion started: 23 July 2026

Open Access Earth System Science Data Discussions

from space, Remote Sens. Environ., 58, 257-266, https://doi.org/10.1016/S0034-4257(96)00067-3, 1996.

Ge, J., Zhang, H., Huang, W., Guo, Z., Xu, L., Xie, Y., Song, M., Ding, Y., and Wang, C.: Plot-Rice v1.0: A global plot-based rice benchmark dataset with spatiotemporal heterogeneity for scientific deep learning, Int. J. Appl. Earth Obs. Geoinf., 140, 104569, https://doi.org/10.1016/j.jag.2025.104569, 2025.

Golden, C. D., Childs, M. L., Mudele, O. E., Andriamizarasoa, F. A., Bouley, T. A., De Nicola, G., Fontaine, M. A., Huybers, P. J., Mahatante, P. T., and Rabemananjara, R.: Climate-smart public health for global health resilience, Lancet Planet. Health, 9, 101293, https://doi.org/10.1016/j.lanplh.2025.101293, 2025.

Golden, C. D., Zamborain-Mason, J., Levis, A., Rice, B. L., Allen, L. H., Hampel, D., Hazen, J., Metcalf, C. J. E., Randriamady, H. J., and Shahab-Ferdows, S.: Prevalence of micronutrient deficiencies across diverse environments in rural Madagascar, Front. Nutr., 11, 1389080, https://doi.org/10.3389/fnut.2024.1389080, 2024.

Gorelick, N., Hancher, M., Dixon, M., Ilyushchenko, S., Thau, D., and Moore, R.: Google Earth Engine: Planetary-scale geospatial analysis for everyone, Remote Sens. Environ., 202, 18-27, https://doi.org/10.1016/j.rse.2017.06.031, 2017.

Jiang, J., Zhang, H., Ge, J., Zuo, L., Xu, L., Song, M., Ding, Y., Xie, Y., and Huang, W.: The 20 m Africa rice distribution map of 2023, Earth Syst. Sci. Data, 17, 1781-1805, https://doi.org/10.5194/essd-17-1781-2025, 2025.

Jin, Z., Azzari, G., You, C., Di Tommaso, S., Aston, S., Burke, M., and Lobell, D. B.: Smallholder maize area and yield mapping at national scales with Google Earth Engine, Remote Sens. Environ., 228, 115-128, https://doi.org/10.1016/j.rse.2019.04.016, 2019.

Kontgis, C., Schneider, A., and Ozdogan, M.: Mapping rice paddy extent and intensification in the Vietnamese Mekong River Delta with dense time stacks of Landsat data, Remote Sens. Environ., 169, 255-269, https://doi.org/10.1016/j.rse.2015.08.004, 2015.

Kwon, R., Ryu, Y., Ciais, P., Makowski, D., Choi, C., Feng, H., Jeong, S., Tang, P., and Lee, K.: Enabling maize mapping in double-cropping regions of Argentina and Brazil without ground reference data by leveraging multiple satellite platforms, manuscript under review at Int. J. Appl. Earth Obs. Geoinf., 2026.

Kwon, R., Ryu, Y., De Nicola, G., Randriamady, H., Mudele, O. E., Tapera, T., Jo, H., and Golden, C. D.: Annual rice paddy maps of Madagascar at 10 m resolution (2017-2025), version 1.0, Zenodo [data set], https://doi.org/10.5281/zenodo.20654510, 2026.

Kwon, R., Ryu, Y., Lee, K., Tang, P., Choi, C., Jo, S., and Kwak, G.-H.: Operational early-season rice paddy mapping in fragmented smallholder landscapes through gap-filled optical phenology and parcel-based refinement, manuscript under review at Comput. Electron. Agric., 2026.

Li, X. and Yu, L.: Mapping complex cropping patterns in China (2018-2021) at 10 m resolution: A data-driven framework based on multi-product integration and Google Satellite Embedding, Earth Syst. Sci. Data Discuss. [preprint], https://doi.org/10.5194/essd-2025-679, 2025.

Lobell, D. B., Thau, D., Seifert, C., Engle, E., and Little, B.: A scalable satellite-based crop yield mapper, Remote Sens. Environ., 164, 324-333, https://doi.org/10.1016/j.rse.2015.04.021, 2015.

Mantey, S., Attipoe, I., and Alhassan, A.: A comparative analysis of satellite imagery for land cover classification: Evaluating Google Satellite Embeddings, Sentinel-2, and Landsat-8 data with

https://doi.org/10.5194/essd-2026-518
Preprint. Discussion started: 23 July 2026

XGBoost, Research Square [preprint], https://doi.org/10.21203/rs.3.rs-7961146/v1, 2025.

Ni, R., Tian, J., Li, X., Yin, D., Li, J., Gong, H., Zhang, J., Zhu, L., and Wu, D.: An enhanced pixel-based phenological feature for accurate paddy rice mapping with Sentinel-2 imagery in Google Earth Engine, ISPRS J. Photogramm., 178, 282-296, https://doi.org/10.1016/j.isprsjprs.2021.06.018, 2021.

Nishide, A., Shiratori, S., and Doi, K.: Madagascar country profile in food security and nutrition, in: Food Security and Nutrition in Africa: Rural Madagascar, Springer, 17-27, https://doi.org/10.1007/978-981-95-5311-2_2, 2026.

Peel, M. C., Finlayson, B. L., and McMahon, T. A.: Updated world map of the Koppen-Geiger climate classification, Hydrol. Earth Syst. Sci., 11, 1633-1644, https://doi.org/10.5194/hess-11-1633-2007, 2007.

Persello, C. and Bruzzone, L.: Active and semisupervised learning for the classification of remote sensing images, IEEE T. Geosci. Remote, 52, 6937-6956, https://doi.org/10.1109/TGRS.2014.2305805, 2014.

Pettorelli, N., Vik, J. O., Mysterud, A., Gaillard, J.-M., Tucker, C. J., and Stenseth, N. C.: Using the satellite-derived NDVI to assess ecological responses to environmental change, Trends Ecol. Evol., 20, 503-510, https://doi.org/10.1016/j.tree.2005.05.011, 2005.

Potapov, P., Turubanova, S., Hansen, M. C., Tyukavina, A., Zalles, V., Khan, A., Song, X.-P., Pickens, A., Shen, Q., and Cortez, J.: Global maps of cropland extent and change show accelerated cropland expansion in the twenty-first century, Nat. Food, 3, 19-28, https://doi.org/10.1038/s43016-021-00429-z, 2022.

Rigden, A., Golden, C., Chan, D., and Huybers, P.: Climate change linked to drought in Southern Madagascar, npj Clim. Atmos. Sci., 7, 41, https://doi.org/10.1038/s41612-024-00583-8, 2024.

Rigden, A. J., Golden, C., and Huybers, P.: Retrospective predictions of rice and other crop production in Madagascar using soil moisture and an NDVI-based calendar from 2010-2017, Remote Sens., 14, 1223, https://doi.org/10.3390/rs14051223, 2022.

Song, X.-P., Hansen, M. C., Potapov, P., Adusei, B., Pickering, J., Adami, M., Lima, A., Zalles, V., Stehman, S. V., and Di Bella, C. M.: Massive soybean expansion in South America since 2000 and implications for conservation, Nat. Sustain., 4, 784-792, https://doi.org/10.1038/s41893-021-00729-z, 2021.

Tang, P., Ryu, Y., Wang, S., Kwon, R., Lee, K., 2026. A source-free unsupervised domain adaptation framework for large-scale, in-season soybean mapping. ISPRS J. Photogramm. Remote Sens. https://doi.org/10.1016/j.isprsjprs.2026.06.019.

Tucker, C. J.: Red and photographic infrared linear combinations for monitoring vegetation, Remote Sens. Environ., 8, 127-150, https://doi.org/10.1016/0034-4257(79)90013-0, 1979.

Wang, S., Azzari, G., and Lobell, D. B.: Crop type mapping without field-level labels: Random forest transfer and unsupervised clustering techniques, Remote Sens. Environ., 222, 303-317, https://doi.org/10.1016/j.rse.2018.12.026, 2019.

Xiao, X., Boles, S., Frolking, S., Li, C., Babu, J. Y., Salas, W., and Moore III, B.: Mapping paddy rice agriculture in South and Southeast Asia using multi-temporal MODIS images, Remote Sens. Environ., 100, 95-113, https://doi.org/10.1016/j.rse.2005.10.004, 2006.

Xiao, X., Boles, S., Liu, J., Zhuang, D., Frolking, S., Li, C., Salas, W., and Moore III, B.: Mapping paddy rice agriculture in southern China using multi-temporal MODIS images, Remote Sens.

https://doi.org/10.5194/essd-2026-518
Preprint. Discussion started: 23 July 2026

Environ., 95, 480-492, https://doi.org/10.1016/j.rse.2004.12.009, 2005.

Yan, Y. and Ryu, Y.: Exploring Google Street View with deep learning for crop type mapping, ISPRS J. Photogramm., 171, 278-296, https://doi.org/10.1016/j.isprsjprs.2020.11.022, 2021.

Yang, G., Yu, W., Yao, X., Zheng, H., Cao, Q., Zhu, Y., Cao, W., and Cheng, T.: AGTOC: A novel approach to winter wheat mapping by automatic generation of training samples and one-class classification on Google Earth Engine, Int. J. Appl. Earth Obs. Geoinf., 102, 102446, https://doi.org/10.1016/j.jag.2021.102446, 2021.

Yang, J., Hu, Q., Li, W., Song, Q., Cai, Z., Zhang, X., Wei, H., and Wu, W.: An automated sample generation method by integrating phenology domain optical-SAR features in rice cropping pattern mapping, Remote Sens. Environ., 314, 114387, https://doi.org/10.1016/j.rse.2024.114387, 2024.

You, N., Dong, J., Li, J., Huang, J., and Jin, Z.: Rapid early-season maize mapping without crop labels, Remote Sens. Environ., 290, 113496, https://doi.org/10.1016/j.rse.2023.113496, 2023.

Zaheer, S.A., Ryu, Y., Lee, J., Zhong, Z., Lee, K., 2023. In-season wall-to-wall crop-type mapping using ensemble of image segmentation models. IEEE Trans. Geosci. Remote Sens. 61, 1–11. https://doi.org/10.1109/TGRS.2023.3335214.

Zhang, H., Song, M., Ding, Y., Xie, Y., Guo, H., Xu, L., Ge, J., Zhu, Y., Wang, S., and Guo, Z.: GlobalRice20: A 20 m resolution global paddy rice dataset for 2015 and 2024 derived from multi-source remote sensing, Earth Syst. Sci. Data Discuss. [preprint], https://doi.org/10.5194/essd-2026-24, 2026.

Zhao, Z., Dong, J., Zhang, G., Yang, J., Liu, R., Wu, B., and Xiao, X.: Improved phenology-based rice mapping algorithm by integrating optical and radar data, Remote Sens. Environ., 315, 114460, https://doi.org/10.1016/j.rse.2024.114460, 2024.